Brief Communications

Stoichiometry of the Human Glycine Receptor Revealed by Direct Subunit Counting

Nela Durisic,[1,4] Antoine G. Godin,[2] Claudia M. Wever,[4] Colin D. Heyes,[3] Melike Lakadamyali,[1]* and Joseph A. Dent[4]*

[1]Institut de Ciències Fotòniques, 08860 Castelldefels (Barcelona), Spain, [2]Institut universitaire en santé mentale de Québec, Québec, G1J 2G3 Canada, [3]University of Arkansas, School of Chemistry and Biochemistry, Fayetteville, Arkansas 72701, and [4]McGill University, Department of Biology, Montreal, Québec, H3A 1B1 Canada

The subunit stoichiometry of heteromeric glycine-gated channels determines fundamental properties of these key inhibitory neurotransmitter receptors; however, the ratio of α1- to β-subunits per receptor remains controversial. We used single-molecule imaging and stepwise photobleaching in *Xenopus* oocytes to directly determine the subunit stoichiometry of a glycine receptor to be 3α1:2β. This approach allowed us to determine the receptor stoichiometry in mixed populations consisting of both heteromeric and homomeric channels, additionally revealing the quantitative proportions for the two populations.

Introduction

Pentameric glycine receptors (GlyRs) mediate ionotropic inhibitory neurotransmission in the CNS where they play an essential role in inhibition of motor neurons in the spinal cord and brainstem (Aprison and Werman, 1965; Werman et al., 1967). Mutations in glycine receptor subunits cause human hereditary hyperekplexia, a disorder characterized by an exaggerated startle response, which is a consequence of the role of GlyRs in motor reflex circuits of the spinal cord (Bakker et al., 2006). However, GlyRs are widely expressed and contribute to many processes in the CNS, including inflammatory pain perception (Harvey et al., 2004), modulation of auditory and visual pathways (Lynch, 2004), and neurotransmission in the cerebellar cortex (Dieudonné, 1995). Given their diverse functions, GlyRs are potential targets for muscle relaxant, analgesic, anti-inflamatory, and infertility drugs (Webb and Lynch, 2007).

Although GlyRs can form homomeric channels solely composed of α-subunits (α1, α2, or α3 in humans), heteromeric GlyRs composed of both α- and β-subunits mediate most neurotransmission (Grenningloh et al., 1987, 1990; Lynch, 2004, 2009). This is a consequence of the fact that only the β-subunit interacts with gephyrin, a protein important for the synaptic localization of GlyRs (Kirsch et al., 1993; Meyer et al., 1995). Since ligand binding sites are located at GlyR subunit interfaces (Lynch, 2009), understanding GlyR molecular pharmacology requires appropriate knowledge of channel stoichiometry. The subunit stoichiometry will also determine the relative effect of each subunit on fundamental properties of a channel such as single-channel conductance, kinetics of gating, and rate of desensitization (Cooper et al., 1991; Pribilla et al., 1992; Burzomato et al., 2004). Although considerable effort has been devoted to determining the GlyR subunit ratio, the issue still remains unresolved, with a variety of subunit ratios reported (3α1:2β, 2α1:3β, or 1α1:4β) (Langosch et al., 1988; Burzomato et al., 2003; Grudzinska et al., 2005).

The conflicting reports on GlyR subunit ratio reflect the difficulty in determining the *in vivo* stoichiometry of ion channels, mainly due to the limitations of population-based methods, which represent compromises between ease of use, accuracy, and *in vivo* applicability (Langosch et al., 1988; Cooper et al., 1991; Kellenberger et al., 1996; Tretter et al., 1997; Jechlinger et al., 1998; Shapiro and Zagotta, 1998; Baumann et al., 2001; Minier and Sigel, 2004; Grudzinska et al., 2005; Ericksen and Boileau, 2007). Furthermore, the subpopulation of α-homomers can skew measurements of GlyR heteromer stoichiometry when using population-based methods. To overcome these drawbacks, we used single-molecule imaging and stepwise photobleaching of venus fluorescent protein (VFP)-tagged subunits to directly observe and count individual α1- or β-subunits within single GlyR channels (Ulbrich and Isacoff, 2007; Pantoja et al., 2009; Simonson et al., 2010). By determining the photobleaching steps of individual VFPs in both homogenous and heterogenous populations of single channels, we show a subunit ratio of 3α1:2β. Moreover, we quantify the ratio of homomeric and heteromeric channels in a mixed population.

Materials and Methods

Contruction of VFP-tagged channels. A KpnI site was introduced into the intracellular loop of human glycine receptor α1- and β-subunit cDNAs (provided by F. Bedford, McGill University, Quebec, Canada) by overlap extension PCR using the following primer pairs (Integrated DNA Technologies): 5′-GCTCTAGATCACTGGTTGTGGACGTCCTCT-3′ + 5′-

Received April 28, 2012; revised July 16, 2012; accepted July 20, 2012.

Author contributions: N.D., C.D.H., M.L., and J.A.D. designed research; N.D. and C.M.W. performed research; N.D., A.G.G., and C.M.W. analyzed data; N.D., C.D.H., M.L., and J.A.D. wrote the paper.

This work was supported by Fundació Cellex Barcelona. N.D. is a NEST postdoctoral fellow partially supported by the Marie Curie Cofunding of Regional, National and International Programs action of the European Commission. A.G.G. acknowledges support from the CIHR Neurophysics Training Program. C.D.H. acknowledges support from NIH COBRE (5P30RR031154 and 8 P30 GM103450-03). We thank E. Cooper and T. Misgeld for discussions and critical reading of the manuscript.

*M.L. and J.A.D. contributed equally to this work.

The authors declare no financial conflicts of interest.

Correspondence should be addressed to Melike Lakadamyali, Institut de Ciències Fotòniques, Mediterranean Technology Park, 08860 Castelldefels (Barcelona), Spain. E-mail: melike.lakadamyali@icfo.es.

DOI:10.1523/JNEUROSCI.2050-12.2012

Copyright © 2012 the authors 0270-6474/12/3212915-06$15.00/0

CTATGGGATGGTACCAGCCTGTCT-3′ and 5′-GGGGCATATGTACAGCTTCAATACTCTTCG-3′ + 5′-AGACAGGCTGGTACCATCCCATAG-3′ (GlyRα1); 5′-GGGGCATATGAAGTTTTTATTGACAACTGC-3′ + 5′-TCTCTTGGTACCCTTCCAACA-3′; and 5′-GCTCTAGATCATAAATATATAGACCAATATATAAC-3′ + 5′TGTTGGAAGGGTACCAAGAGA-3′ (GlyRβ).

The PCR products were subcloned into the pT7N expression vector using NdeI and XbaI restriction sites. A VFP open reading frame with flanking KpnI sites was generated by PCR amplification of VFP using the primers 5′-GGGGTACCAATGAGTAAAGGAGAAGAA-3′ + 5′-GGTACCGCTTTGTATAGTTCATCCATG-3′.

The VFP PCR product was cloned into pCR2.1-TOPO (Life Technologies) and then subcloned into the pT7N_GlyR construct using the engineered KpnI restriction sites. VFP cDNA was provided by J. Vogel (McGill University, Quebec, Canada).

Expression in Xenopus *oocytes*. The pT7NcDNA constructs were linearized with BamHI or SalI restriction enzymes and capped cRNAs were transcribed using the mMESSAGE mMACHINET7 kit (Life Technologies). Synthesized cRNAs were recovered by LiCl precipitation and resuspended in nuclease-free water at a final concentration of 0.5–1.0 $\mu g\ \mu l^{-1}$.

Xenopus oocytes were provided by I. Vernos (Centre de Regulació Genòmica, Barcelona, Spain) or purchased from NASCO. They were harvested from mature female *Xenopus laevis* according to standard procedures and maintained at 20°C in ND96 solution (Goldin, 1992). Oocytes were injected with 40 nL of cRNA using the Nanoject system (Drummond Scientific) and FemtoJet system (Eppendorf) and incubated for 12–24 h before photobleaching experiments or 1–2 d before electrophysiology. For photobleaching experiments, vitelline envelope and extracellular matrix were removed by incubating the oocytes in 0.05 mg/ml protease K (Roche Applied Science) for 5–6 min immediately before the experiment (Wang, 2004). The oocytes were then allowed to settle on the surface of a chambered coverglass before microscopy. Oocyte electrophysiology was performed as described previously (Putrenko et al., 2005). Judging from the 90% current rise time of channels exposed to 5 mM glycine, the 90% perfusion rate is <15 ms, consistent with previous reports (Madeja et al., 1991). Data were acquired at 1 kHz using Clampex software (Molecular Devices). Dose–response curves were fit to the Hill equation using Igor Pro (Wave Metrics) to estimate EC_{50} and Hill coefficients. Picrotoxin was purchased from Sigma Aldrich. Currents at saturating concentrations of glycine ranged from 0.8 to 2.4 μA with no significant difference in the maximum current of tagged and untagged channels. We never saw glycine responses in water-injected control oocytes.

Data acquisition. Images were acquired on a total internal reflection fluorescence (TIRF) microscope fitted with a 100× 1.4 NA oil-immersion objective. Excitation light at 488 nm (0.5 mW at the sample plane) from an argon–krypton laser (Coherent) was used to excite VFP. The emission of VFP was collected with a BP 525/50 emission filter (Chroma Technology) and recorded onto an EMCCD camera (Andor Technology) with an exposure time of 100 ms. We started acquisition of movies before turning the laser on to avoid pre-photobleaching of VFP.

Data analysis. Typically, we observed ~50–120 single channels over one field of view (40 × 40 μm) from 20 to 80 s long movies. A square region of 3 × 3 pixels around the center of each spot was chosen to extract intensity–time traces using ImageJ. We excluded from our analysis: spots that did not appear in the first frame recorded after the excitation laser was turned on, spots that moved by more than one pixel before they photobleached, spots that were fluorescent for only one frame, and multiple partially overlapping spots (~17% of α:β-VFP and ~27% of α-VFP:β traces discarded).

The steps in intensity–time traces were counted manually. Photobleaching steps were defined as events in which the mean intensity of the smallest step was at least twice the standard deviation of the background fluorescence. The steps within each single trace were similar in amplitude, but varied between different traces. This is a consequence of the Gaussian profile of the laser and complex topology of the oocyte membrane, which results in different local illumination intensities of the evanescent field.

Determination of probability to observe n *photobleaching steps in a time trace.* When the subunit stoichiometry of the receptor is constant, the observed distribution of steps should follow the binomial distribution given by the following:

$$q_n = \left(\frac{M!}{n!(M-n)!}\right) P^n (1-P)^{M-n}, \quad (1)$$

where q_n is the probability to observe n steps in a time trace, M is the total number of subunits, n is the observed number of steps, and P is the probability for VFP to be fluorescent. For example, for two subunits, the above expression reduces to a series of three equations: $q_2 = P^2$ (probability for two steps), $q_1 = 2P(1-P)$ (probability for one step), and $q_0 = (1-P)^2$ (probability for completely dark channels).

Similarly, in a mixture of two populations of channels, the distribution of observed steps is a sum of two binomial distributions:

$$q_n^{2\ populations} = f_1 \cdot q_n(M_1, P) + f_2 \cdot q_n(M_2, P), \quad (2)$$

where M_1 and M_2 are the total number of subunits labeled in each channel type and f_1 and f_2 are fractions of each population.

The probability, P, for the VFP to be fluorescent can be estimated by directly fitting the observed number of steps to Equations 1 or 2, or the probability can be set as a parameter in the same equations, reducing the number of variables in the fit. In this study, we used a least square fit with a Levenberg–Marquard algorithm to obtain the parameters for each fit model. Finally, we estimated the goodness of fit for each model used with the χ^2 test. A low value of χ^2 (or $p > 0.05$) indicates a good fit of the model to the data, whereas a high value of χ^2 (or $p < 0.05$) indicates that the model does not fit the data.

Calculation of missed events. We determined the photon distribution for a single VFP from β-VFP traces that showed two photobleaching steps. We calculated the step size for each step by subtracting the average intensity of step 1 from step 2, or the average background intensity from step 1. The resulting distribution of step sizes could be fit with a Gaussian with mean of 23.3 and standard deviation of 6.3 intensity counts. Because of the random nature of photobleaching, there is a finite probability that more than one VFP would photobleach within the same acquisition frame. This would result in one larger photobleaching step and underestimating the total number of photobleaching steps. We determined missed events as traces that contained steps larger than 46.6 counts (twice the mean single step size). In α:β-VFP channels, we found ~6% traces containing missed events. In case of α-VFP:β and α-VFP homomeric channels, the same correction was applied to recover one missed event in a trace. For these cases, there is a small possibility that more than two VFPs would photobleach within the same imaging frame. Those traces were discarded due to higher uncertainty in recovering the correct number of steps.

Results

Subunits tagged with fluorescent proteins form functional channels

To visualize GlyR subunits within individual channels, we inserted VFP into the intracellular loop between transmembrane domains TM3 and TM4 of human GlyR α1- and β-subunits and expressed them in *Xenopus* oocytes (Fig. 1*A*). Determinants of subunit association are in the *N*-terminal extracellular domains of the α- and β-subunits and therefore tagging the intracellular loop should not affect channel stoichiometry (Kuhse et al., 1993). To confirm that the VFP-tagged GlyR subunits form functional channels, we analyzed subunits expressed in *Xenopus* oocytes by two-electrode voltage-clamp. We fitted normalized glycine concentration–response relationships to the Hill equation and found that the EC_{50} was only modestly altered even when both α1- and β-subunits were tagged simultaneously (Table 1). Similarly, the Hill coefficient, which reflects both the cooperativity of ligand binding and the number of ligand molecules that must bind to activate the channel, was well conserved in tagged and untagged

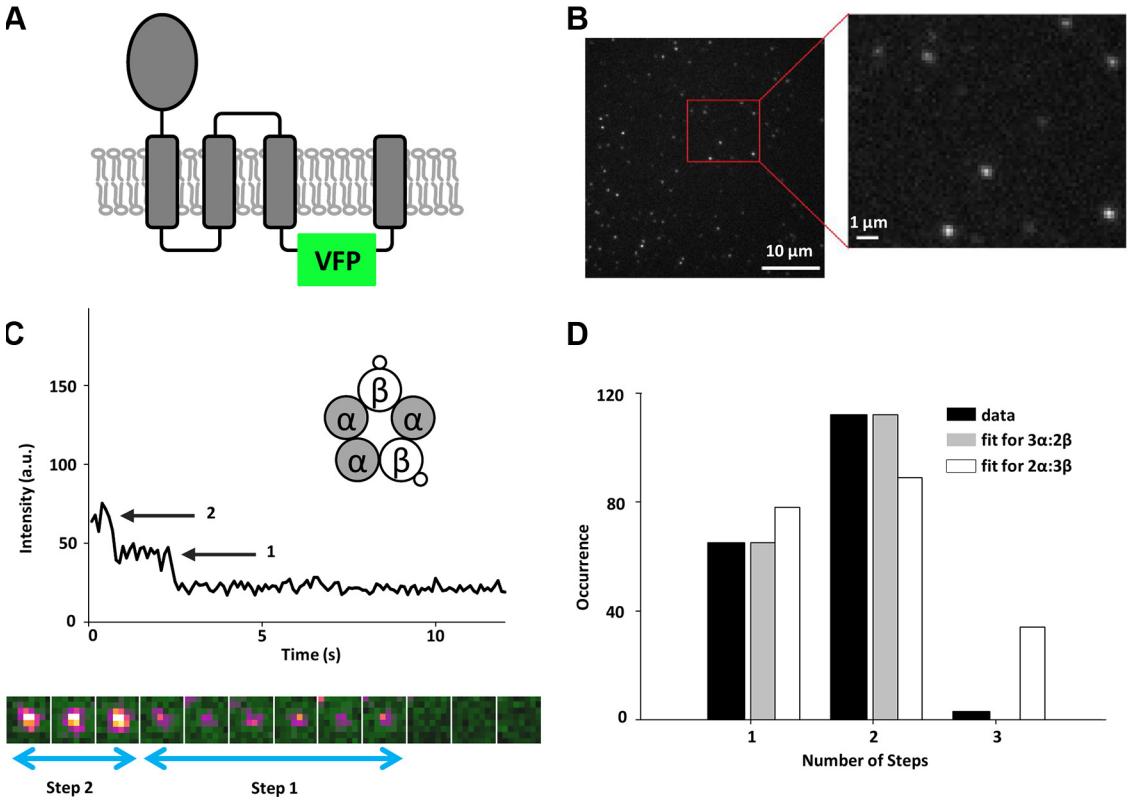

Figure 1. β-subunit stoichiometry of GlyR. ***A***, Placement of the VFP in the intracellular loop between TM3 and TM4 transmembrane domains. ***B***, An example of the first frame from a movie of a *Xenopus* oocyte plasma membrane expressing single GlyR channels. The expression level is low enough that the probability for two channels to coincide within the same diffraction-limited spot is small, as shown in the high-magnification region. ***C***, Representative intensity–time trace showing two photobleaching steps. Transfection scheme with β-VFP and untagged α-subunits is shown in the inset. Below the graph, 10 images corresponding to the channel from which the time trace was extracted are shown in pseudocolor. When the first VFP photobleaches, the color of a channel changes from yellow to magenta. Photobleaching of the second VFP results in a change from magenta to green (background). Box size is 1.1 × 1.3 μm. ***D***, Histogram of photobleaching steps counted from intensity–time traces after correction for missed events (black bars), and the best fits to the binomial distribution for two (dark gray bars) and three (white bars) β-subunits. The fit to three β-subunits is poor ($p < 0.01$) and gives a low percentage of fluorescent VFP (50%).

Table 1. EC_{50} and Hill coefficients obtained by two-electrode voltage clamp when untagged or VFP-tagged GlyR α− and β-subunits were expressed in *Xenopus* oocytes

Subunit composition	EC_{50} (μM)	Hill coefficient	*N* (oocytes)
GlyRα	303.8 ± 20.4	1.28 ± 0.09	5
GlyRα-FP	266.2 ± 27.4	1.1 ± 0.1	4
GlyRα; GlyRβ	357.9 ± 22.5	1.5 ± 0.1	5
GlyRα-FP; GlyRβ	473.7 ± 24.3	1.5 ± 0.1	5
GlyRα; GlyRβ-FP	408.5 ± 22.2	1.5 ± 0.1	6
GlyRα-FP; GlyRβ-FP	331.1 ± 15.6	1.54 ± 0.09	6

Values are mean ± SEM.

Table 2. The expected distributions for the number of steps calculated using the binomial distribution for different scenarios of channel stoichiometry

	Steps				
	1	2	3	4	5
β-VFP					
Data	36%	62%	2%	0%	0%
Expected for 2 β-subunits and $p = 78\%$	36%	64%	0%	0%	0%
Expected for 3 β-subunits and $p = 78\%$	11%	41%	48%	0%	0%
α-VFP					
Data	18%	30%	43%	6%	3%
Expected for 3 α-subunits, $p = 78\%$, homomers = 15%	9%	36%	44%	6%	5%
Expected for 2 α-subunits, $p = 78\%$, homomers = 15%	31%	55%	3%	6%	5%

The probability for VFP to be fluorescent was set as 78%. In the case of α1-VFP:β channels, the percentage of homomers was additionally set as 15%. Comparison of data with different scenarios of heteromeric GlyR stoichiometry.

channels (Table 1), indicating that the allosteric properties of the channel were not substantially affected by the VFP-tag. Finally, we showed that the VFP-tagged β-subunit confers picrotoxin resistance on the heteromeric receptor (IC_{50} = 79.5 ± 3.8 μM picrotoxin in the heteromer vs 4.6 ± 0.2 μM for the homomer, $n = 4$ each), similar to that conferred by the untagged β-subunit (Pribilla et al., 1992). Based on these results, we concluded that VFP-tagged subunits formed fully functional channels with properties similar to those of native channels.

Single heteromeric channels contain two β-subunits

We first injected *Xenopus* oocytes with an equimolar ratio of cRNA of β-VFP and untagged α1-subunit, which allowed us to visualize only the β-subunits within heteromeric channels, since the α1-only homomers were nonfluorescent. For low expression levels of channels, we could visualize, using TIRF microscopy, VFP-tagged subunits as mostly immobile, diffraction-limited spots within the membrane of the oocyte (Fig. 1*B*).

To count β-subunits, we extracted intensity–time traces from each diffraction-limited spot, which showed stepwise photobleaching behavior (Fig. 1*C*). Of 180 spots, 76 photobleached in one step, 101 showed two steps, and three showed three photobleaching steps. These data are consistent with GlyRs composed of two β-subunits per channel. The negligible percentage of traces (1.6%) that showed three photobleaching steps is likely due

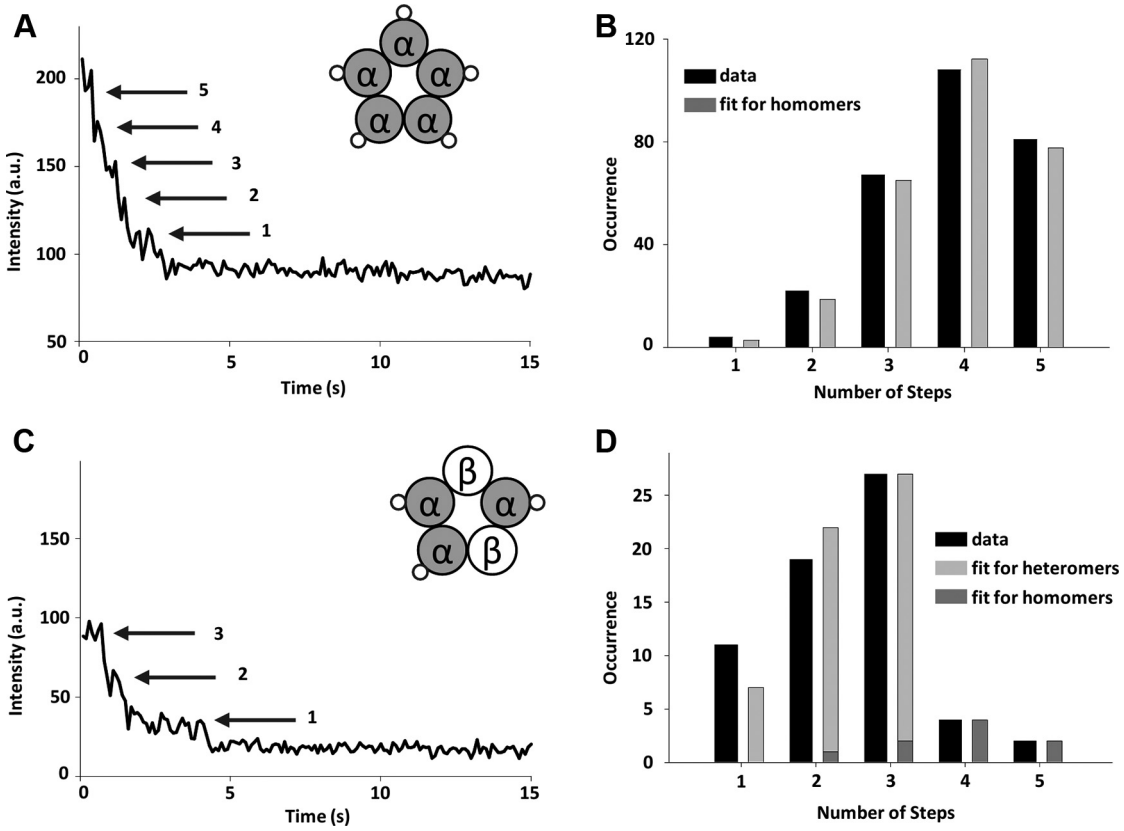

Figure 2. α-subunit stoichiometry of GlyR. ***A***, Representative intensity–time trace showing photobleaching steps observed in a homomeric GlyR channel. Five steps are clearly visible (arrows). ***B***, Histogram of the number of photobleaching steps counted from intensity–time traces (black bars) after correction for missed events and the best fit to the binomial distribution for five subunits (gray bars) (goodness of fit, $p = 0.82$). ***C***, Representative intensity–time trace showing three photobleaching steps observed in heteromeric channels where α1-subunit is labeled. Inset, Proposed composition of the heteromer. ***D***, Histogram of the number of photobleaching steps counted from intensity–time traces after correction for missed events (black bars) in a mixed population of homomeric and heteromeric channels and the binomial distribution for three subunits (light gray bars) and five subunits (dark gray bars). The gray bars are calculated from the best fit to the data, in which the proportion of homomeric and heteromeric channels and the probability for the VFP to be fluorescent were left as free parameters (goodness of fit, $p = 0.52$). The corresponding observed and calculated percentage of traces that show one to five photobleaching steps are given in Table 2.

to overlapping channels within one spot (Ulbrich and Isacoff, 2007). The single-step photobleaching events are in part due to missed events, in which two VFPs photobleached within a single frame and therefore could not be resolved. We corrected for missed events by characterizing the photon distribution of single steps (see Materials and Methods, above). After this correction, the remaining single-step photobleaching events were likely due to misfolding or incomplete maturation of the VFP that resulted in dark proteins. The resulting distribution of number of steps fit well with a binomial distribution for two β-subunits per channel, given that 78% of the VFP population is fluorescent (see Materials and Methods, above; Fig. 1*D*), which is consistent with other fluorescent protein (FP) variants (~80% for GFP) (Ulbrich and Isacoff, 2007). We also tested the possibility that our data could be consistent with GlyRs containing three β-subunits per channel, a proposed stoichiometry from previous bulk studies (Grudzinska et al., 2005). Our data fits poorly to this scenario (best fit with $\chi^2 = 36.4$, $p < 0.01$; Fig. 1*D*) and we recover a much lower percentage (~50%) for the VFP to be fluorescent (for a comparison of data with expected results for different channel stoichiometry scenarios, see Table 2). Given these results, our data strongly suggests that heteromeric GlyRs contain two β-subunits per channel.

To rule out an effect of the relative expression level of each subunit on the observed stoichiometry, we examined a case in which we strongly biased the transfection ratio toward the β-subunit. We varied the ratio of α:β-VFP cRNA from 1:1 to 1:3 and consistently found that channels with only two β-subunits were formed ($n = 56$ or 64% for two steps and $n = 31$ or 36% for one step) while the percentage of fluorescent VFP stayed unchanged (78%). We therefore conclude that the stoichiometry of the heteromeric human GlyR channel is preserved and that there are two β-subunits per channel.

Determination of α1-subunit stoichiometry in mixed populations of homomeric and heteromeric channels

To test the ability of our single-step photobleaching approach to detect up to five subunits, we expressed VFP-tagged α1-subunits alone in *Xenopus* oocytes. As demonstrated by electrophysiology, α1-subunits form functional homomeric channels (Table 1), which are known to be pentameric (Langosch et al., 1988). The intensity–time traces showed up to five photobleaching steps (Fig. 2*A*) and the distribution of the counted steps fit well ($\chi^2 = 1.55$, $p = 0.82$) to a binomial distribution for five subunits with 78% probability for VFP to be fluorescent (Fig. 2*B*). The fact that the population of fluorescent VFP was identical when all the subunits were tagged shows that folding and maturation of the fluorescent proteins were not affected by specific subunit tagging or labeling density.

For additional confirmation of the GlyR channel stoichiometry, we next determined the number of α1-subunits within heteromeric channels. In oocytes transfected with α1-VFP and

untagged β-subunit, we expect to visualize two populations: homopentamers consisting only of α1-subunits and heteropentamers with labeled α1- and unlabeled β-subunits. We strongly biased the amount of cRNA toward β-subunit (transfection ratio of 1:3) to suppress the expression of homomeric channels. Figure 2*C* shows a typical example of an intensity–time trace with three steps. The largest number of photobleaching steps counted per trace was five, but traces predominantly showed two and three photobleaching steps (Fig. 2*D*, black bars). The data fit best ($\chi^2 = 3.21$, $p = 0.52$) to the sum of two binomial distributions corresponding to three α1-subunits (heteromers; Fig. 2*D*, light gray bars) and five α1-subunits (homomers; Fig. 2*D*, dark gray bars). The probability of VFP to be fluorescent, which was left as a free parameter of the fit, was found to be 77%, consistent with the heteromeric and homomeric channels shown above. This result further confirms the 3α1:2β stoichiometry of the heteromeric GlyR channels and strongly disagrees with alternative reports for two α1-subunits per channel (Table 2). Furthermore, our data provide a quantitative estimate of the homomeric and heteromeric populations, with the majority of the channels (85%) being heteromeric, as expected.

Discussion

Accurate determination of ion channel subunit composition and stoichiometry *in vivo* is relevant for understanding channel function and developing effective therapeutic agents (Webb and Lynch, 2007; Lynch, 2009). Determining the stoichiometry of GlyR presents a particular challenge because the background population of α-homomers frustrates population-based assays. In this study, using specific labeling and counting of GlyR subunits in single channels, we could directly determine the heteromeric channel stoichiometry. This approach was possible because the *Xenopus* oocytes do not endogenously express the human GlyR receptor, so we could specifically tag individual subunits with FPs such that there is a one-to-one correspondence between the number of FPs and subunits. Our results clearly demonstrate a stoichiometry of 3α1:2β for heteropentameric GlyRs and show that this stoichiometry is independent of the expression levels of individual subunits. Our approach can be used to accurately determine stoichiometry even in heterogenous populations consisting of a combination of homomeric and heteromeric channels, and to estimate the proportion of each population. These results demonstrate the power of single-protein counting by stepwise photobleaching, a method that is applicable to a number of other important ion channels.

3α1:2β stoichiometry for heteromeric GlyRs has several implications for GlyR function and pharmacology. First, the β-subunits bind gephyrin, the intracellular protein necessary for localization of GlyRs to the synapse (Meyer et al., 1995). The number of β-subunits per channel that are available to bind gephyrin presumably affects gephyrin stoichiometry, which in turn may affect channel clustering and localization. Second, the homomer to heteromer ratio when α- and β-subunits are coexpressed suggests that there is not a strong bias toward association of α with β during channel assembly in oocytes. An interesting question is whether factors besides the relative affinity of α-subunits for β-subunits account for the proportion of extrasynaptic α-homomers *in vivo* (Turecek and Trussell, 2002; Deleuze et al., 2005). Third, α-subunit homomers form functional glycine receptors and therefore α–α-subunit interfaces can bind glycine and gate GlyRs. Homomeric GlyRs are thought to be presynaptic while heteromeric GlyRs are synaptic (Kirsch et al., 1993; Turecek and Trussell, 2001, 2002; Deleuze et al., 2005). It could be useful to develop drugs that specifically target presynaptic over postsynaptic channels or vice versa. However, a 3α1:2β heteromer stoichiometry indicates that the heteromer also has at least one α–α-subunit interface. If that α–α interface is sufficient to bind glycine and gate the heteromer, it would cast doubt on the likelihood of developing a homomer-specific agonist. Similarly, in cells that coexpress α1-, α3-, and β-subunits, the stoichiometry of α1 and α3 within a single channel could influence screens for analgesic compounds affecting the α3-containing GlyRs in the dorsal horn (Harvey et al., 2004). With the accurate determination of stoichiometry in the GlyR channels, we can now begin to address these questions.

References

Aprison MH, Werman R (1965) The distribution of glycine in cat spinal cord and roots. Life Sci 4:2075–2083.

Bakker MJ, van Dijk JG, van den Maagdenberg AM, Tijssen MA (2006) Startle syndromes. Lancet Neurol 5:513–524.

Baumann SW, Baur R, Sigel E (2001) Subunit arrangement of gamma-aminobutyric acid type A receptors. J Biol Chem 276:36275–36280.

Burzomato V, Groot-Kormelink PJ, Sivilotti LG, Beato M (2003) Stoichiometry of recombinant heteromeric glycine receptors revealed by a pore-lining region point mutation. Receptors Channels 9:353–361.

Burzomato V, Beato M, Groot-Kormelink PJ, Colquhoun D, Sivilotti LG (2004) Single-channel behavior of heteromeric α1β glycine receptors: an attempt to detect a conformational change before the channel opens. J Neurosci 24:10924–10940.

Cooper E, Couturier S, Ballivet M (1991) Pentameric structure and subunit stoichiometry of a neuronal nicotinic acetylcholine receptor. Nature 350:235–238.

Deleuze C, Runquist M, Orcel H, Rabié A, Dayanithi G, Alonso G, Hussy N (2005) Structural difference between heteromeric somatic and homomeric axonal glycine receptors in the hypothalamo-neurohypophysial system. Neuroscience 135:475–483. 10.1016/j.neuroscience.2005.05.024.

Dieudonné S (1995) Glycinergic synaptic currents in Golgi cells of the rat cerebellum. Proc Natl Acad Sci U S A 92:1441–1445.

Ericksen SS, Boileau AJ (2007) Tandem couture: cys-loop receptor concatamer insights and caveats. Mol Neurobiol 35:113–128.

Goldin AL (1992) Maintenance of Xenopus laevis and oocyte injection. Methods Enzymol 207:266–279.

Grenningloh G, Rienitz A, Schmitt B, Methfessel C, Zensen M, Beyreuther K, Gundelfinger ED, Betz H (1987) The strychnine-binding subunit of the glycine receptor shows homology with nicotinic acetylcholine receptors. Nature 328:215–220.

Grenningloh G, Schmieden V, Schofield PR, Seeburg PH, Siddique T, Mohandas TK, Becker CM, Betz H (1990) Alpha subunit variants of the human glycine receptor: primary structures, functional expression and chromosomal localization of the corresponding genes. EMBO J 9:771–776.

Grudzinska J, Schemm R, Haeger S, Nicke A, Schmalzing G, Betz H, Laube B (2005) The beta subunit determines the ligand binding properties of synaptic glycine receptors. Neuron 45:727–739.

Harvey RJ, Depner UB, Wässle H, Ahmadi S, Heindl C, Reinold H, Smart TG, Harvey K, Schütz B, Abo-Salem OM, Zimmer A, Poisbeau P, Welzl H, Wolfer DP, Betz H, Zeilhofer HU, Müller U (2004) GlyR alpha3: an essential target for spinal PGE2-mediated inflammatory pain sensitization. Science 304:884–887.

Jechlinger M, Pelz R, Tretter V, Klausberger T, Sieghart W (1998) Subunit composition and quantitative importance of hetero-oligomeric receptors: GABAA receptors containing alpha6 subunits. J Neurosci 18:2449–2457.

Kellenberger S, Eckenstein S, Baur R, Malherbe P, Buhr A, Sigel E (1996) Subunit stoichiometry of oligomeric membrane proteins: GABAA receptors isolated by selective immunoprecipitation from the cell surface. Neuropharmacology 35:1403–1411.

Kirsch J, Wolters I, Triller A, Betz H (1993) Gephyrin antisense oligonucleotides prevent glycine receptor clustering in spinal neurons. Nature 366:745–748.

Kuhse J, Laube B, Magalei D, Betz H (1993) Assembly of the inhibitory glycine receptor: identification of amino acid sequence motifs governing subunit stoichiometry. Neuron 11:1049–1056.

Langosch D, Thomas L, Betz H (1988) Conserved quaternary structure of ligand-gated ion channels: the postsynaptic glycine receptor is a pentamer. Proc Natl Acad Sci U S A 85:7394–7398.

Lynch JW (2004) Molecular structure and function of the glycine receptor chloride channel. Physiol Rev 84:1051–1095.

Lynch JW (2009) Native glycine receptor subtypes and their physiological roles. Neuropharmacology 56:303–309. 10.1016/j.neuropharm.2008.07.034.

Madeja M, Musshoff U, Speckmann EJ (1991) A concentration-clamp system allowing two-electrode voltage-clamp investigations in oocytes of *Xenopus laevis*. J Neurosci Methods 38:267–269.

Meyer G, Kirsch J, Betz H, Langosch D (1995) Identification of a gephyrin binding motif on the glycine receptor beta subunit. Neuron 15:563–572.

Minier F, Sigel E (2004) Techniques: use of concatenated subunits for the study of ligand-gated ion channels. Trends Pharmacol Sci 25:499–503.

Pantoja R, Rodriguez EA, Dibas MI, Dougherty DA, Lester HA (2009) Single-molecule imaging of a fluorescent unnatural amino acid incorporated into nicotinic receptors. Biophys J 96:226–237.

Pribilla I, Takagi T, Langosch D, Bormann J, Betz H (1992) The atypical M2 segment of the beta subunit confers picrotoxinin resistance to inhibitory glycine receptor channels. EMBO J 11:4305–4311.

Putrenko I, Zakikhani M, Dent JA (2005) A family of acetylcholine-gated chloride channel subunits in *Caenorhabditis elegans*. J Biol Chem 280:6392–6398.

Shapiro MS, Zagotta WN (1998) Stoichiometry and arrangement of heteromeric olfactory cyclic nucleotide-gated ion channels. Proc Natl Acad Sci U S A 95:14546–14551.

Simonson PD, Deberg HA, Ge P, Alexander JK, Jeyifous O, Green WN, Selvin PR (2010) Counting bungarotoxin binding sites of nicotinic acetylcholine receptors in mammalian cells with high signal/noise ratios. Biophys J 99:L81–83.

Tretter V, Ehya N, Fuchs K, Sieghart W (1997) Stoichiometry and assembly of a recombinant GABAA receptor subtype. J Neurosci 17:2728–2737.

Turecek R, Trussell LO (2001) Presynaptic glycine receptors enhance transmitter release at a mammalian central synapse. Nature 411:587–590.

Turecek R, Trussell LO (2002) Reciprocal developmental regulation of presynaptic ionotropic receptors. Proc Natl Acad Sci U S A 99:13884–13889.

Ulbrich MH, Isacoff EY (2007) Subunit counting in membrane-bound proteins. Nat Methods 4:319–321.

Wang MH (2004) A technical consideration concerning the removal of oocyte vitelline membranes for patch clamp recording. Biochem Biophys Res Commun 324:971–972.

Webb TI, Lynch JW (2007) Molecular pharmacology of the glycine receptor chloride channel. Curr Pharm Des 13:2350–2367.

Werman R, Davidoff RA, Aprison MH (1967) Inhibition of motoneurones by iontophoresis of glycine. Nature 214:681–683.